NANO LETTERS

pubs.acs.org/NanoLett

Embedded Binary Eutectic Alloy Nanostructures: A New Class of Phase Change Materials

S. J. Shin,[†,‡] J. Guzman,[†,‡] C.-W. Yuan,[†,‡,||] Christopher Y. Liao,[†,‡] Cosima N. Boswell-Koller,[†,‡] P. R. Stone,[†,‡] O. D. Dubon,[†,‡] A. M. Minor,[†,§] Masashi Watanabe,[§,⊥] Jeffrey W. Beeman,[‡] K. M. Yu,[‡] J. W. Ager III,[‡] D. C. Chrzan,[*,†,‡] and E. E. Haller[†,‡]

[†]Department of Materials Science and Engineering, University of California, Berkeley, California 94720 and [‡]Materials Sciences Division and [§]National Center for Electron Microscopy, Lawrence Berkeley National Laboratory, Berkeley, California 94720

ABSTRACT Phase change materials are essential to a number of technologies ranging from optical data storage to energy storage and transport applications. This widespread interest has given rise to a substantial effort to develop bulk phase change materials well suited for desired applications. Here, we suggest a novel and complementary approach, the use of binary eutectic alloy nanoparticles embedded within a matrix. Using GeSn nanoparticles embedded in silica as an example, we establish that the presence of a nanoparticle/matrix interface enables one to stabilize both nanobicrystal and homogeneous alloy morphologies. Further, the kinetics of switching between the two morphologies can be tuned simply by altering the composition.

KEYWORDS phase change, eutectic, information storage, semiconductor nanocrystals, GeSn

Phase change materials are essential components of both optical data storage and the emerging static random access memory (RAM) technologies.[1] The prototypical materials used in these applications are in the alloy family typified by $Ge_2Sb_2Te_5$. These alloys can exist at room temperature in either a stable crystalline state or a metastable amorphous state, and, ideally, either an optical (e.g., reflectance) or electrical (e.g., resistance) property is markedly different between the two states. Also important is the ability to switch rapidly between the states using, for example, a tailored current pulse.[2] There is a substantial current research effort dedicated to understanding existing phase change materials,[3−6] and to identify new materials with improved properties.[7−9] The focus of these studies is mostly on identifying those properties that make a single, bulk material suitable for phase change applications. Here, we demonstrate a new approach that is based upon the size and composition dependence of equilibrium and kinetic aspects of phase transformations. Our approach exploits the unique properties of eutectic binary alloys that emerge when they are embedded within nanoscale volumes: When mixed Ge−Sn nanocrystals are formed within amorphous SiO_2, the nanocrystals exhibit a bilobed structure expected for strongly segregating binary alloys.[10] However, rapid cooling following pulsed laser melting stabilizes a metastable, amorphous, compositionally mixed state at room temperature. Moderate heating followed by slower cooling returns the nanocrystals to their initial bilobed, crystalline state.

It is well-known that the presence of a solid/solid interface at the surface of an embedded nanocrystal provides additional degrees of control over the properties of nanocrystals.[11−13] For example, in contrast to the melting point depression expected for free-standing nanocrystals[14] Ge nanocrystals embedded in amorphous silica exhibit a melting point elevation of nearly 200 K above the bulk value. Moreover, after melting, the system can be supercooled 200 K below the bulk value.[15] The potential for a single material to be supercooled and superheated is a direct result of the embedded nanoscale volumes and is not expected within a bulk material.[16]

The unusual kinetics of phase transformations at the nanoscale enables a broad range of phenomena beyond tuning the melting and solidification points. For example, we have found that heating Ge nanocrystals embedded in amorphous silica with a properly tuned laser pulse, that is, pulsed-laser melting (PLM), transforms the nanocrystals to an amorphous state.[17] As a subsequent annealing restores the crystalline state, this suggests that embedded nanocrystals can function as a phase change material.

Alloying offers the possibility to engineer further the phase-change properties of embedded nanocrystals. It is well-known that in bulk eutectic alloys the melting point of the alloy can be substantially lower than that of elemental

* To whom correspondence should be addressed. E-mail: dcchrzan@berkeley.edu.

|| Present address: Department Biologie II, Ludwig-Maximilians-Universitat, Munchen, Germany.

⊥ Present address: Department of Materials Science and Engineering, Lehigh University, Bethlehem, PA, 18105.

Received for review: 02/24/2010
Published on Web: 00/00/0000

DOI: 10.1021/nl100670r | *Nano Lett.* **XXXX,** *xxx,* 000–000

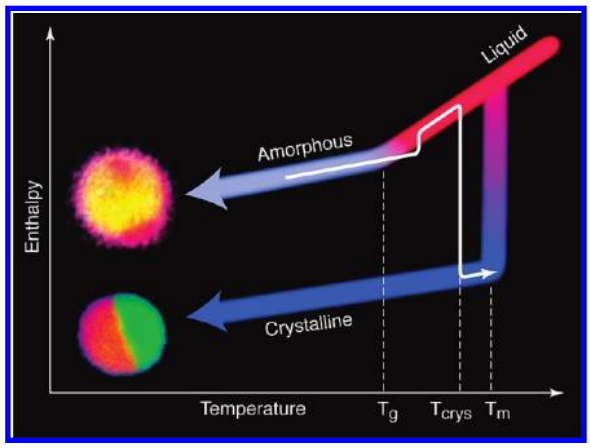

FIGURE 1. A schematic of the operating principle of the proposed phase change nanostructures. Enthalpy curves are sketched for the liquid, crystalline and amorphous phases. Above T_m, the melting point for bilobed nanocrystal, the entire nanocluster is liquid. As it cools, it may follow one of two paths. If the cooling rate is slow, the equilibrium path (red to dark blue) will be followed, yielding the equilibrium bilobed structure, a half crystalline metallic/half crystalline semiconductor nanostructure. If the cooling rate is rapid (red to light blue), the liquid will at first be supercooled, and then will solidify into the amorphous state with nearly homogeneous composition at T_g. Upon heating, the amorphous state may follow the path indicated by the white arrow and crystallize at a temperature T_{crys}.[33] Each of the temperatures can be varied experimentally. T_g depends on cooling rate. Varying the composition changes T_{crys}. The melting point, T_m, also varies with composition. Thus embedded nanoscale structures offer the opportunity to tune both thermodynamics and kinetics to obtain optimal transition characteristics for technological applications.

phases of either component. Further, metals are known to influence the recrystallization temperature of amorphous thin films.[18,19] The implication is that alloying may offer the opportunity to tune further phase equilibria and transition kinetics at the nanoscale, and thereby enable the development of a new type of phase-change material: binary eutectic-alloy nanostructures (BEANs).

Figure 1 illustrates conceptually the envisioned behavior. Heating an embedded BEAN to above its melting point yields a liquid droplet with a homogeneous composition. Upon cooling, two types of paths are accessible. (1) For slow cooling, the BEAN can crystallize at temperature T_m, leading to the equilibrium bilobed structure. (2) For rapid cooling, the liquid can supercool, then freeze at temperature T_g into an amorphous structure with homogeneous composition. Upon reheating, the amorphous structure can recrystallize at temperature T_{crys}. Each of the relevant temperatures can be tuned by altering the composition, the cooling rate, or both.

To explore experimentally the potential for BEANs to serve as phase change materials, we fabricated GeSn nanocrystals. In the bulk, the GeSn system displays eutectic behavior with the eutectic composition very near to pure Sn, but a melting point very slightly suppressed from that of pure Sn, 231.97 to 231.1 °C.[20] Ge and Sn are strongly segregating and each individually forms nanocrystals within silica. Both can be introduced easily into silica using ion implantation, a chemically clean, well-tested and understood,[21,22] and technologically relevant process.

GeSn nanocrystals embedded in silica are formed by sequential implantation of Sn and Ge followed by annealing for 1 h at 900 °C. The composition of the nanocrystals is tuned by changing the ratio of implanted species. Figure 2a shows an energy-filtered transmission electron microscopy (EFTEM) image of as-formed $Ge_{0.67}Sn_{0.33}$ (Ge/Sn = 2:1) nanocrystals (see details in Supporting Information for detailed description of implantation procedure). The nanocrystals in Figure 2a–c have an average radius of 13 ± 4 nm, values typical for all of the compositions considered. (These measurements represent a coarse estimate of the characteristics of our size distribution. See the online Supporting Information for details.) The nanocrystals are clearly phase separated into Ge and Sn regions, forming a bilobed morphology. High-resolution electron microscopy suggests that the lobes are crystalline (Supporting Information Figure S2).

A single pulse from an excimer laser is used to melt the alloy nanocrystals (PLM). At the laser wavelength and pulse energy fluence used, 248 nm (5 eV) and 0.3 J/cm^2, respectively, the particles absorb the laser energy and melt while the silica matrix stays relatively unaffected. This leads to very rapid cooling and results in an amorphous phase with nearly homogeneous composition.

Figure 2b shows an EFTEM image of the Ge/Sn embedded nanoclusters after PLM. The bilobed structure characteristic of the equilibrium morphology are no longer present. In addition, there appear to be a large number of small nanoclusters about each larger nanocluster.

More moderate heating and a less rapid cooling should return the nanoclusters to their equilibrium morphology. Indeed this is the case. As shown in Figure 2c, after a rapid thermal annealing (RTA) treatment of the mixed nanoclusters at 400 °C for 10 s, the initial bilobed geometry is restored, demonstrating that the transformation is reversible.

The properties of the mixed phase are likely to be very different from that of the bilobed crystalline state. We have conducted both X-ray energy dispersive spectroscopy (XEDS) and extended X-ray absorption fine structure (EXAFS) experiments to determine the composition and local environment of the bilobed and mixed structures (Supporting Information Figures S3–S5, Table S1).

XEDS indicates that the mixing of elemental species within the mixed phase is nearly uniform. EXAFS measurements of bond lengths and coordination numbers also suggest that the mixed-composition material is amorphous. In situ TEM-based electron energy loss spectroscopy (EELS) analysis show that the plasmon resonance for the mixed phase lies between that of nanocrystalline Ge and nanocrystalline Sn (Supporting Information Figure S6). Since this plasmon energy is determined by the valence electron density, we conclude that the valence electron density of the PLM structure lies between that of

DOI: 10.1021/nl100670r | *Nano Lett.* **XXXX,** *xxx,* 000–000

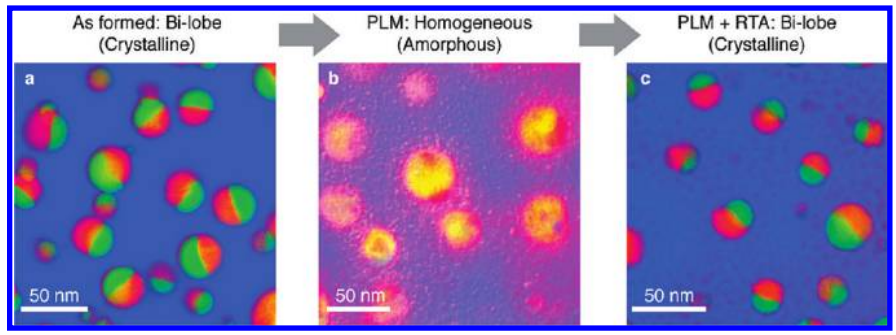

FIGURE 2. Phase maps of phase-changed $Ge_{0.67}Sn_{0.33}$ nanoclusters. Phase maps are constructed for phase-changed $Ge_{0.67}Sn_{0.33}$ nanoclusters.(Ge/Sn = 4:2) phase-specific featured spectra extracted from EFTEM spectrum imaging data set are used to map phases in the images. Green represents Sn, red represents Ge, and blue represents SiO_2. Yellow represents a mixture of Sn and Ge. The nanocrystals transform from (a) equilibrium Ge−Sn bilobed structure in their as-formed state to (b) metastable Ge−Sn mixture with nearly homogeneous composition after PLM process, and back to (c) equilibrium Ge−Sn bilobed structure upon moderate heating at 400 °C for 10 s followed by slow cooling.

the Ge and Sn structures. Taken together, these observations suggest that the post-PLM structure of the nanoclusters is close to a homogeneously mixed amorphous GeSn alloy, and they confirm that our phase change experiments follow a crystalline−amorphous−crystalline path.

Having established that one can induce a phase change within BEANs, we turn our attention to controlling the transformation. In particular, we consider how the composition can be used to alter recrystallization kinetics and thereby tune the recrystallization temperature.

Starting with amorphized nanoclusters, we applied a 10 s rapid thermal annealing at various temperatures and monitored the degree of crystallization using ex situ Raman spectroscopy. Figure 3a shows typical Raman spectra obtained from $Ge_{0.8}Sn_{0.2}$ nanoclusters as a function of RTA temperature. As expected, the post-PLM sample shows a broad Raman signal similar to that of an amorphous Ge thin film.[23] In contrast, the as-formed nanocrystals show the Raman peak expected for Ge nanocrystals, including the expected asymmetry due to their small size. At low RTA temperatures (e.g., the 323 °C spectrum in Figure 3a), the Raman peak is intermediate in width between the as-formed and amorphous cases and is starting to develop the characteristic asymmetry to lower frequency typical of nanocrystals. This indicates the formation of small crystalline Ge clusters. As the RTA temperature increases, the peak narrows and eventually resembles that of the as-formed state, showing that larger Ge clusters have recrystallized. We can, therefore, use the full width at half-maximum (fwhm) of the Raman peak to characterize the extent of the observed recrystallization.

Figure 3b displays the fwhm (scaled by the fwhm at 25 °C for each data set) plotted as a function of RTA temperature for nanocrystals of differing compositions. The lines are guides to the eye, constructed by fitting the data to an empirical functional form (Supporting Information). We define the characteristic recrystallization temperature, the point for which the fwhm is reduced by one-half of its total reduction upon complete recrystallization, to be T_{crys}. These temperatures are plotted versus composition in Figure 3c.

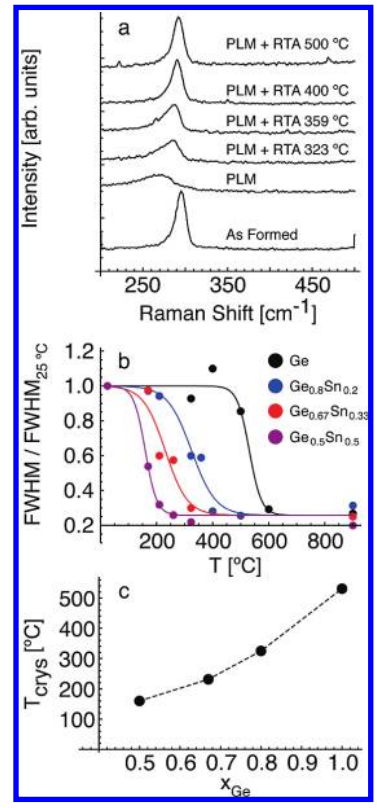

FIGURE 3. Temperature dependent crystallization of amorphized $Ge_{1-x}Sn_x$ nanoclusters. The full width at half-maximum (fwhm) of the crystalline Ge Raman peak at ~300 cm^{-1} is used to monitor the recrystallization of the BEANs. (a) RTA temperature dependent ex situ Raman spectra of amorphized $Ge_{0.8}Sn_{0.2}$ nanocrystals. After PLM, the Raman spectrum is nearly identical to that of an amorphous Ge film.[24] As the annealing temperature increases, the Raman peak sharpens, converging to the spectrum of the as-formed nanocrystals at 400 °C. (b) Plot of the fwhm of the Raman peak vs temperature for different compositions. The lines are fits of the data to an empirical form and serve as a guide to the eye (Supporting Information). The fitted lines enable estimation of T_{crys}, defined to be the inflection point in the fitted curve. (c) T_{crys} versus composition in atomic percent as estimated from (b). The dashed line is a guide for the eye.

For pure Ge nanoclusters, recrystallization begins near 500 °C and reaches completion around 600 °C. This is in

DOI: 10.1021/nl100670r | *Nano Lett.* **XXXX,** *xxx,* 000–000

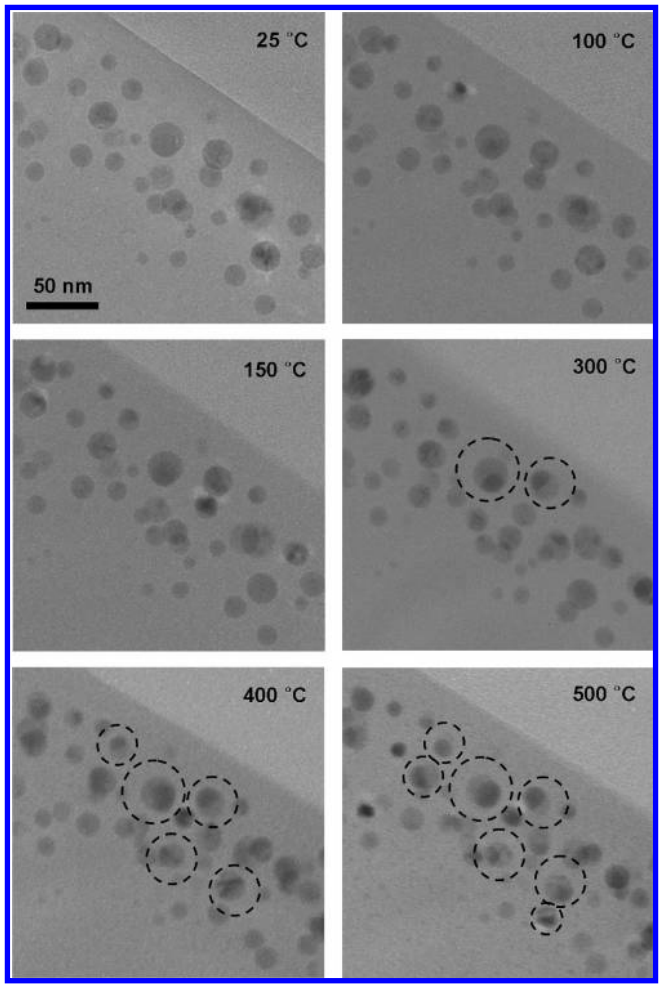

FIGURE 4. In situ TEM micrographs of amorphized $Ge_{0.8}Sn_{0.2}$ (x = 0.2) nanoclusters at elevated temperature. Images of the same sample region at elevated temperatures are captured to investigate the evolution of nanoclusters from the homogeneously mixed amorphous phase to the bilobed crystalline phase. BEANs with a dashed circles show clear phase separation between Ge and Sn phases. Note that some overlapped, but still single phase nanocrystals can be also observed at low temperatures (<150 °C).

good agreement with the reported recrystallization temperature (T_{crys}) of amorphous Ge/SiO_2 superlattices with 5 nm thickness.[24] As the Sn composition, x, is increased, T_{crys} of $Ge_{1-x}Sn_x$ decreases. For example, T_{crys} is lowered to approximately 150 °C in nanoclusters with composition near 50 atomic percent Sn (Ge/Sn = 1:1).

TEM in situ heating was employed to observe directly the recrystallization process of amorphized $Ge_{0.8}Sn_{0.2}$ (Ge/Sn = 4:1) nanoclusters. Images captured as a function of temperature are shown in Figure 4. Since the initial structure is in a homogeneously mixed amorphous state, each nanocluster is in a single phase as represented by single contrast. Phase separated bilobed nanocrystals can be first observed at 300 °C, and most of the phase segregation occurs between 300 and 400 °C. These temperatures are in excellent agreement with the data plotted in Figure 3 that indicate $T_{crys} \approx$ 325 °C for $Ge_{0.8}Sn_{0.2}$.

The observed dependence of the recrystallization temperature on Sn content merits discussion. It is well-known that amorphous semiconductors, such as Si and Ge, crystallize at temperatures well below the normal crystallization temperature when in contact with metals.[18,19] This phenomenon, known as metal-induced crystallization, has been observed for both semiconductor-metal bilayer structures,[25−28] and codeposited composites.[29,30] Evidently, GeSn nanocrystals embedded in silica display a similar phenomenon. Certainly, the recrystallization is influenced by the number of GeSn bonds in the structure. Although the precise origins of the composition dependence of T_{crys} remain to be understood, we note that the observed tuning range extends from near room temperature to over 500 °C.

Looking ahead to the applications of BEANs to data storage, we note that at this time, it is not possible to characterize directly the transport properties of the bilobed and amorphous nanostructures. However, the resistivities of amorphous Ge films and intrinsic crystalline Ge differ by 3 orders of magnitude[31] and there is theoretical evidence that the band gap of $Ge_{1-x}Sn_x$ can be reduced substantially from that of pure Ge.[32] Thus we expect that the transport and optical properties of the amorphous PLM structure will be different from those of the bilobed structure, and further that these differences can be tuned through choice of composition.

Acknowledgment. We thank Allyson Aranda and Erik Nelson for their expert support at Stanford Synchrotron Radiation Laboratory (SSRL). This work was supported by the Director, Office of Science, Office of Basic Energy Sciences, Division of Materials Sciences and Engineering, of the U.S. Department of Energy under Contract No. DE-AC02-05CH11231. SJS acknowledges support from NSF IGERT program. J.G. was supported by the Berkeley Graduate Fellowship and U.S. NSF Grant Nos. DMR-0405472 and DMR-0902179. P. R. S. acknowledges fellowship support from the National Science Foundation. Electron microscopy experiments were conducted at the National Center for Electron Microscopy, Lawrence Berkeley National Laboratory, which is supported by the U.S. Department of Energy under Contract No. DE-AC02-05CH11231. EXAFS experiments were carried out at SSRL, a national user facility operated by Stanford University on behalf of the U.S. Department of Energy, Office of Basic Energy Sciences.

Supporting Information Available. Detailed descriptions of the nanocrystals synthesis procedures, EFTEM spectrum imaging technique, HRTEM images analysis, HAADF-STEM imaging with XEDS analysis, EXAFS measurements and analysis, EELS spectra analysis, Raman data fitting method, RBS data, and particle size analysis. This material is available free of charge via the Internet at http://pubs.acs.org.

REFERENCES AND NOTES

(1) Wuttig, M.; Yamada, N. Phase-change materials for rewriteable data storage. *Nat. Mater.* **2007**, *6*, 824–832.
(2) Ovshinsky, S. R. Reversible Electrical Switching Phenomena in Disordered Structures. *Phys. Rev. Lett.* **1968**, *21*, 1450–1453.

DOI: 10.1021/nl100670r | *Nano Lett.* **XXXX,** *xxx,* 000–000

(3) Caravati, S.; Bernasconi, M.; Kuhne, T. D.; Krack, M.; Parrinello, M. Unravelling the Mechanism of Pressure Induced Amorphization of Phase Change Materials. *Phys. Rev. Lett.* **2009**, *102*, 205502.

(4) Shportko, K.; et al. Resonant bonding in crystalline phase-change materials. *Nat. Mater.* **2008**, *7*, 653–658.

(5) Kim, S.; Drza, L. T. High latent heat storage and high thermal conductive phase change materials using exfoliated graphite nanoplatelets. *Sol. Energy Mater. Sol. Cells* **2009**, *93*, 136−142.

(6) Krebs, D.; et al. Threshold field of phase change memory materials measured using phase change bridge devices. *Appl. Phys. Lett.* **2009**, *95*, 082101.

(7) Lencer, D.; et al. A map for phase-change materials. *Nat. Mater.* **2008**, *7*, 972–977.

(8) Wang, S. L.; et al. Phase-change memory devices based on gallium-doped indium oxide. *Appl. Phys. Lett.* **2009**, *94*, 113503.

(9) Welnic, W.; Wuttig, M. Reversible switching in phase-change materials. *Mater. Today* **2008**, *11*, 20–27.

(10) Yuan, C. W.; et al. Structure map for embedded binary alloy nanocrystals. *Appl. Phys. Lett.* **2008**, *93*, 193114.

(11) Sutter, E.; Sutter, P. Phase diagram of nanoscale alloy particles used for vaporliquid-solid growth of semiconductor nanowires. *Nano Lett.* **2008**, *8*, 411–414.

(12) Holmberg, V. C.; Panthani, M. G.; Korgel, B. A. Phase Transitions, Melting Dynamics, and Solid-State Diffusion in a Nano Test Tube. *Science* **2009**, *326*, 405–407.

(13) Kim, B. J.; et al. Kinetics of Individual Nucleation Events Observed in Nanoscale Vapor-Liquid-Solid Growth. *Science* **2008**, *322*, 1070–1073.

(14) Pawlow, P. The dependency of the melting point on the surface energy of a solid body. *Z. Phys. Chem* **1909**, *65*, 545−548.

(15) Xu, Q.; et al. Large melting-point hysteresis of Ge nanocrystals embedded in SiO_2. *Phys. Rev. Lett.* **2006**, *97*, 209902.

(16) Landau, L. D.; Lifshitz, E. M. *Statistical Physics*, 3rd ed.; Pergamon Press: Elmsford, NY, 1980; Vol. 5, Part 1.

(17) Shin, S. J., Guzman, J., Yuan, C.-W., Liao, C. Y., Stone, P. R., Dubon, O. D., Minor, A. M., Watanabe, M., Ager III, J. W., Chrzan, D. C. & Haller, E. E. Structural Characterization of GeSn Alloy Nanocrystals Embedded in SiO_2, in *Electron Crystallography for Materials Research and Quantitative Characterization of Nanostructured Materials*. eds Moeck, P., Hovmoeller, S., Nicolopoulos, S., Rouvimov, S., Petkov, V., Gateshki, M. & Fraundorf, P. (Materials Research Society Symposium Proceedings Volume 1184, Warrendale, PA, 2009) HH04−08.

(18) Oki, F.; Ogawa, Y.; Fujiki, Y. Effect of Deposited Metals on Crystallization Temperature of Amorphous Germanium Film. *Jpn. J. Appl. Phys.* **1969**, *8*, 1056.

(19) Herd, S. R.; Chaudhari, P.; Brodsky, M. H. Metal contact induced crystallization in films of amorphous silicon and germanium. *J. Non-Cryst. Solids* **1972**, *7*, 309–327.

(20) Balde, L.; Legendre, B.; Balkhi, A. Equilibrium Diagram of Phases of the Ternary-System Germanium-Tin Tellurium. *J. Alloys Compd.* **1995**, *216*, 285–293.

(21) Yuan, C. W.; et al. Theory of Nanocluster Size Distributions from Ion Beam Synthesis. *Phys. Rev. Lett.* **2009**, *102*, 146101.

(22) Yuan, C. W.; et al. Size distribution evolution of ion-beam-synthesized nanoclusters in silica. *Phys. Rev. B* **2009**, *80*, 134121.

(23) Sharp, I. D.; et al. Stable, freestanding Ge nanocrystals. *J. Appl. Phys.* [Online early access]. DOI:Artn 124316.

(24) Williams, G. V. M.; Bittar, A.; Trodahl, H. J. Crystallization and Diffusion in Progressively Annealed a-Ge/SiO_x Superlattices. *J. Appl. Phys.* **1990**, *67*, 1874–1878.

(25) Konno, T. J.; Sinclair, R. Crystallization of Silicon in Aluminum Amorphous-Silicon Multilayers. *Philos. Mag. B* **1992**, *66*, 749–765.

(26) Wang, Z. M.; Wang, J. Y.; Jeurgens, L. P. H.; Phillipp, F.; Mittemeijer, E. J. Origins of stress development during metal-induced crystallization and layer exchange: Annealing amorphous Ge/crystalline Al bilayers. *Acta Mater.* **2008**, *56*, 5047–5057.

(27) Nast, O.; Hartmann, A. J. Influence of interface and Al structure on layer exchange during aluminum-induced crystallization of amorphous silicon. *J. Appl. Phys.* **2000**, *88*, 716–724.

(28) Edelman, F.; Komem, Y.; Bendayan, M.; Beserman, R. Initial Crystallization Stage of Amorphous-Germanium Films. *J. Appl. Phys.* **1992**, *72*, 5153–5157.

(29) Tan, Z. Q.; Heald, S. M.; Rapposch, M.; Bouldin, C. E.; Woicik, J. C. Gold-Induced Germanium Crystallization. *Phys. Rev. B* **1992**, *46*, 9505–9519.

(30) Radnoczi, G.; Robertsson, A.; Hentzell, H. T. G.; Gong, S. F.; Hasan, M. A. Al Induced Crystallization of a-Si. *J. Appl. Phys.* **1991**, *69*, 6394–6399.

(31) Nath, P.; Dutta, V.; Chopra, K. L. Effects of Alloying on the Transport Properties of Amorphous and Crystalline Ge Films. *J. Phys. C: Solid State Phys.* **1979**, *12*, L203–L208.

(32) Alberi, K.; et al. Band anticrossing in highly mismatched Sn_xGe_{1-x} semiconducting alloys. *Phys. Rev. B* **2008**, *77*, 073202.

(33) Kasap, S. O.; Capper, P. *Handbook of Electronic and Photonic Materials*; Springer: New York, 2006; p 1406.

DOI: 10.1021/nl100670r | *Nano Lett.* **XXXX,** *xxx,* 000–000